Supporting information for

Temperature- and pressure-induced phase transitions in the metal formate framework of $[ND_4][Zn(DCOO)_3]$ and $[NH_4][Zn(HCOO)_3]$

Mirosław Mączka,*[,†] Paweł Kadłubański,[†] Paulo Tarso Cavalcante Freire,[‡] Bogusław Macalik,[†] Waldeci Paraguassu,[§] Krysztof Hermanowicz,[†] and Jerzy Hanuza[†]

[†]*Institute of Low Temperature and Structure Research, Polish Academy of Sciences, Box 1410, 50-950 Wrocław 2, Poland*

[‡]*Departamento de Física, Universidade Federal do Ceará, P.O. Box 6030, 60455-970, Fortaleza-CE, Brazil*

[§]*Departamento de Física, Universidade Federal do Pará, 66075-110, Belém, PA, Brazil*

*E-mail: m.maczka@int.pan.wroc.pl

Table S1. The correlation diagram showing the correspondence between the optical modes in the *P6₃22* and *P6₃* structures of $[NH_4][Zn(HCOO)_3]$ ($[ND_4][Zn(DCOO)_3]$) (the data for the *P6₃* structure are given in parentheses).

ion	vibration	Free ion symmetry	Site symmetry	Factor group symmetry
HCOO-		**C_{2v}**	**C_2 (C_1)**	**D_6 (C_6)**
	ν_1, ν_2 or ν_3	A_1	A (A)	$A_1+B_1+E_1+E_2$ ($3A+3B+3E_1+3E_2$)
	ν_4, ν_5 or ν_6	B_1	B (A)	$A_2+B_1+E_1+E_2$ ($3A+3B+3E_1+3E_2$)
	T’	$A_1 + B_1 + B_2$	A+2B (3A)	$A_1+2A_2+B_1+2B_2+3E_1+3E_2$ ($9A+9B+9E_1+9E_2$)
	L	$A_2 + B_1 + B_2$	A+2B (3A)	$A_1+2A_2+B_1+2B_2+3E_1+3E_2$ ($9A+9B+9E_1+9E_2$)
NH_4^+ (ND_4^+)		**T_d**	**D_3 (C_3)**	**D_6 (C_6)**
	ν_1	A_1	A_1 (A)	(3A+3B)
	ν_2	E	E (E)	($3E_1+3E_2$)
	ν_3, ν_4	F_2	A_2+E (A+E)	($3A+3B+3E_1+3E_2$)
	T’	F_2	A_2+E (A+E)	($3A+3B+3E_1+3E_2$)
	L	F_1	A_2+E (A+E)	($3A+3B+3E_1+3E_2$)
Zn^{2+}			**D_3 (C_1)**	**D_6 (C_6)**
			A_2 (A)	A_2+B_1 (3A+3B)
			E (2A)	E_1+E_2 ($3E_1+3E_2$)

Table S2. Calculated IR and Raman wavenumbers (ν , cm^{-1}), infrared intensities (I_{IR}, km mol^{-1}), and Raman intensities (I_R, relative) for two model compounds: the NH_4^+ (ND_4^+) cation in the dimeric complex unit (model 1) and the monomeric $[Zn(HCOO)_6]^{4-}$ ($[Zn(DCOO)_6]^{4-}$) unit (model 2). X denotes H or D, and the values for deuterated units are listen in parentheses.

B3LYP			Mode description[a]	
ν	I_{IR}	I_R	Model 1	Model 2
3556 (2604)	60.5 (93.3)	62.5 (36.2)	ν(NX) : $\nu_3(NX_4)$	
3352 (2436)	233.3 (140.9)	48.6 (33.0)	ν(NX) : $\nu_3(NX_4)$	
3142 (2341)	849.5 (397.3)	277.3 (116.3)	ν(NX) : $\nu_3(NX_4)$	
2877 (2002)	1044.8 (578.0)	99.9 (68.0)	ν(NX) : $\nu_1(NX_4)$	
2826 (2078)	302.8 (232.3)	9.0 (7.2)		ν(C-X): $\nu_1(XCOO^-)$
2825 (2076)	96.7 (69.9)	136.4 (80.1)		ν(C-X): $\nu_1(XCOO^-)$
2823 (2074)	388.6 (284.3)	33.6 (15.9)		ν(C-X): $\nu_1(XCOO^-)$
2821 (2072)	50.2 (51.8)	187.78 (83.2)		ν(C-X): $\nu_1(XCOO^-)$
2813 (2066)	182.4 (130.8)	186.4 (93.5)		ν(C-X): $\nu_1(XCOO^-)$
2811 (2065)	136.7 (83.2)	76.4 (46.8)		ν(C-X): $\nu_1(XCOO^-)$
1740 (1245)	2.1 (23.0)	10.0 (1.5)	$\gamma_s(NX_2)$: $\nu_2(NX_4)$	
1735 (1729)	13.6 (14.2)	1.2 (0.8)		ν(C-O): $\nu_4(XCOO^-)$
1730 (1219)	10.8 (16.9)	3.1 (3.1)	$\delta_s(NX_2)$: $\nu_2(NX_4)$	
1696 (1686)	1409.2 (1302.2)	0.02 (0.5)		ν(C-O): $\nu_4(XCOO^-)$
1695 (1686)	1207.8 (1562.5)	0.2 (0.3)		ν(C-O): $\nu_4(XCOO^-)$
1693 (1684)	1586.7 (1715.8)	0.06 (0.02)		ν(C-O): $\nu_4(XCOO^-)$
1687 (1676)	101.9 (81.0)	0.2 (1.3)		ν(C-O): $\nu_4(XCOO^-)$
1685 (1674)	194.2 (121.7)	0.3 (1.0)		ν(C-O): $\nu_4(XCOO^-)$
1537 (1170)	229.4 (93.9)	4.0 (0.4)	$\delta(NX_3)$: $\nu_4(NX_4)$	
1518 (1113)	82.1 (22.8)	2.2 (2.2)	$\gamma(NX_3)$: $\nu_4(NX_4)$	

1465 (1083)	85.7 (32.7)	1.2 (0.6)	$\gamma(NX_3) : \nu_4(NX_4)$	
1413 (1036)	3.7 (0.5)	5.8 (16.1)		$\delta(XCO): \nu_5(XCOO^-)$
1410 (1035)	103.7 (12.8)	3.4 (3.4)		$\delta(XCO): \nu_5(XCOO^-)$
1408 (1035)	46.5 (17.9)	18.7 (0.9)		$\delta(XCO): \nu_5(XCOO^-)$
1408 (1035)	69.4 (21.7)	12.7 (8.8)		$\delta(XCO): \nu_5(XCOO^-)$
1406 (1034)	58.0 (6.2)	17.7 (7.6)		$\delta(XCO): \nu_5(XCOO^-)$
1405 (1034)	24.0 (16.8)	17.6 (6.9)		$\delta(XCO): \nu_5(XCOO^-)$
1369 (1348)	165.5 (89.4)	20.0 (29.2)		$\nu(C\text{-}O): \nu_2(XCOO^-)$
1368 (1347)	151.2 (121.3)	8.1 (2.8)		$\nu(C\text{-}O): \nu_2(XCOO^-)$
1366 (1346)	259.5 (14.8)	2.9 (45.4)		$\nu(C\text{-}O): \nu_2(XCOO^-)$
1364 (1345)	19.6 (201.7)	24.3 (5.3)		$\nu(C\text{-}O): \nu_2(XCOO^-)$
1363 (1343)	19.3 (96.9)	33.7 (17.2)		$\nu(C\text{-}O): \nu_2(XCOO^-)$
1363 (1343)	111.7 (29.2)	23.3 (12.7)		$\nu(C\text{-}O): \nu_2(XCOO^-)$
1074 (922)	3.4 (8.0)	1.8 (0.9)		$\gamma\ (C\text{-}H): \nu_6(HCOO^-)$
1074 (922)	3.2 (4.3)	2.9 (0.4)		$\gamma\ (C\text{-}X): \nu_6(XCOO^-)$
1067 (918)	0.3 (3.0)	3.9 (1.0)		$\gamma\ (C\text{-}X): \nu_6(XCOO^-)$
1067 (918)	5.5 (8.1)	2.0 (0.6)		$\gamma\ (C\text{-}X): \nu_6(XCOO^-)$
1065 (916)	4.1 (7.2)	3.0 (0.9)		$\gamma\ (C\text{-}X): \nu_6(XCOO^-)$
1064 (916)	1.0 (3.1)	3.3 (0.8)		$\gamma\ (C\text{-}X): \nu_6(XCOO^-)$
768 (760)	28.4 (48.4)	3.3 (5.0)		$\gamma\ (C\text{-}O): \nu_3(XCOO^-)$
768 (760)	48.5 (28.7)	5.0 (3.4)		$\gamma\ (C\text{-}O): \nu_3(XCOO^-)$
766 (758)	52.8 (39.6)	0.08 (0.8)		$\gamma\ (C\text{-}O): \nu_3(XCOO^-)$
766 (758)	1.0 (1.8)	4.5 (4.7)		$\gamma\ (C\text{-}O): \nu_3(XCOO^-)$
765 (758)	39.9 (51.1)	0.8 (0.2)		$\gamma\ (C\text{-}O): \nu_3(XCOO^-)$
764 (756)	2.2 (2.1)	0.4 (0.12)		$\gamma\ (C\text{-}O): \nu_3(XCOO^-)$

613 (434)	5.6 (0.6)	1.5 (1.1)	$L(NX_4)$	
401 (348)	15.1 (17.8)	2.8 (0.9)	$L(NX_4)$	
248 (239)	13.8 (11.1)	0.9 (0.3)	$L(NX_4)$	
221 (219)	8.0 (5.8)	3.1 (3.2)		ν(Zn-O)
217 (214)	56.3 (59.7)	0.0 (0.01)		ν(Zn-O)
215 (188)	90.3 (28.3)	0.4 (0.4)	$T'(NX_4)$	
214 (211)	53.3 (53.9)	0.05 (0.04)		$T'(XCOO^-)$*ν(Zn-O)
206 (204)	53.3 (61.1)	0.8 (0.7)		$T'(XCOO^-)$*δ(OZnO)
201 (197)	26.2 (24.1)	1.1 (0.9)		$T'(XCOO^-)$*δ(OZnO)
189 (186)	13.7 (15.4)	1.2 (1.1)		$T'(XCOO^-)$*ν(Zn-O)
186 (184)	11.3 (7.9)	1.9 (1.8)		$T'(XCOO^-)$*ν(Zn-O)
176 (174)	72.6 (71.6)	0.8 (0.5)		$T'(XCOO^-)$*ν(Zn-O)
166 (165)	83.3 (78.2)	0.0 (0.01)		$T'(XCOO^-)$*ν(Zn-O)
158 (156)	34.5 (28.0)	0.6 (0.7)		$T'(XCOO^-)$*δ(OZnO)
147 (143)	22.8 (19.0)	0.8 (0.5)		$L(XCOO^-)$*δ(ZnOC)
144 (139)	2.9 (1.5)	0.6 (0.5)		$L(XCOO^-)$*δ(ZnOC)
137 (132)	18.5 (17.7)	1.3 (0.9)		$L(XCOO^-)$*δ(ZnOC)
132 (128)	12.5 (8.3)	0.12 (0.02)		$L(XCOO^-)$*ν(Zn-O)
127 (123)	9.3 (7.1)	0.4 (0.6)		$L(XCOO^-)$
120 (114)	13.1 (10.0)	0.8 (0.3)		$L(XCOO^-)$
114 (171)	32.9 (76.3)	0.4 (0.11)	$T'(NX_4)$	
110 (97)	26.8 (26.9)	6.1 (3.4)		$L(XCOO^-)$
107 (116)	25.8 (19.5)	0.8 (0.3)	$T'(NX_4)$	
103 (92)	4.5 (4.2)	2.6 (2.5)		$L(XCOO^-)$
92 (84)	20.8 (4.1)	0.9 (1.2)		$L(XCOO^-)$
87 (83)	0.9 (15.8)	2.0 (0.9)		$L(XCOO^-)$

87 (80)	2.4 (8.5)	2.1 (1.6)	$L(XCOO^-)$
86 (78)	5.9 (0.2)	2.4 (1.9)	$L(XCOO^-)$
76 (71)	0.04 (0.2)	2.6 (1.7)	$L(XCOO^-)$
69 (67)	0.01 (2)	0.3 (0.2)	$L(XCOO^-)*T'(XCOO^-)$
61 (59)	0.9 (0.6)	2.4 (2.6)	$L(XCOO^-)*T'(XCOO^-)$
59 (57)	0.12 (0.03)	0.2 (0.11)	$L(XCOO^-)*T'(XCOO^-)$
50 (48)	0.02 (0.01)	2.0 (1.92)	$L(XCOO^-)*T'(XCOO^-)$
44 (41)	0.2 (0.3)	3.6 (3.3)	$L(XCOO^-)*T'(XCOO^-)$
40 (38)	0.1 (0.2)	1.4 (1.5)	$L(XCOO^-)*T'(XCOO^-)$
36 (34)	0.06 (0.2)	0.2 (0.1)	$L(XCOO^-)*T'(XCOO^-)$
32 (30)	0.6 (0.9)	0.3 (0.4)	$L(XCOO^-)*T'(XCOO^-)$
27 (26)	0.01 (0.01)	1.4 (1.2)	$L(XCOO^-)*T'(XCOO^-)$
26 (25)	0.0 (0.01)	0.9 (0.9)	$L(XCOO^-)*T'(XCOO^-)$

[a] Abbreviations: as, asymmetric; s, symmetric; ν, stretching; δ, in-plane bending; γ out-of-plane bending; τ, torsion; ω, wagging; ρ, rocking.

Table S3. Experimental IR and Raman frequencies (in cm^{-1}) of $[NH_4][Zn(HCOO)_3]$ and $[ND_4][Zn(DCOO)_3]$ and suggested assignments.[a] X denotes H or D.

$[NH_4][Zn(HCOO)_3]$				$[ND_4][Zn(DCOO)_3]$				Assignment
Raman 295 K	Raman 5 K	IR 295 K	IR 5 K	Raman 295 K	Raman 5 K	IR 295 K	IR 5 K	
		3337w	3380m, 3374m, 3371m,		2507vw	2483m	2508m, 2497sh	$\nu_3(NX_4^+)$
	3164vw, 3117w	3162m	3150m, 3138sh			2371m, 2336m	2359w, 2327m 2308m	$\nu_3(NX_4^+)$
	3022w	3025m	3033m, 3020m				2258sh	$\nu_1(NX_4^+)$
2970w	2973w	2974s	2962sh		2230w	2247m	2238m	$\nu_3(NX_4^+)$
	2950w	2946m	2944s				2219m	$\nu_3(NX_4^+)$
2891m	2897m	2887m	2896s	2189m	2197m	2189m	2197m, 2187m	$\nu_1(XCOO^-)$
	2854w, 2845w	2847m	2856s, 2845s	2126w	2155w	2154m	2156m, 2137w	$\nu_3(NX_4^+)$
1677vw	1705vw, 1686vw	1690sh	1690w			1126w	1156w, 1147w 1129w	$\nu_2(NX_4^+)$
1567vw	1567vw	1576vs	1575vs			1572s	1571s	$\nu_4(XCOO^-)$
1448vw 1429vw	1464vw, 1447vw, 1442w	1440m	1464m, 1450w 1439m	1083vw	1084vw	1084m	1114m, 1098w 1083m	$\nu_4(NX_4^+)$
1380s	1391w, 1381s	1382s	1390vw, 1382s 1378vw	1024m	1023m	1021s	1023s, 1019s	$\nu_5(XCOO^-)$
1371s	1372s, 1359w 1352w	1368s	1372s, 1366s	1342s	1350w, 1344s	1342s	1352w, 1344s 1338w	$\nu_2(XCOO^-)$
						1204w	1209w,1190w	combination bands

1075w	1074w, 1078w					913w	914w	$\nu_6(XCOO^-)$
809sh, 803w	806w, 813w	804m	808m	795w	799w	796s	808sh, 800s	$\nu_3(XCOO^-)$
		286m	329m, 311m		296vw	287m	305s, 301s	T'(Zn^{2+}) and L(NX_4^+)
			301s					
		257m	283s, 269s			241m	263m, 250m, 246s	T'(Zn^{2+}) and L(NX_4^+)
			259s				241sh	
244w	277vw, 266w			245m	262w, 251w, 240w			T'($XCOO^-$) and T'(Zn^{2+})
	245w							
		226m	238s			223m	231m	T'($XCOO^-$)
	213w, 202w	202m	215w, 206s				206w, 190s, 201m	T'($XCOO^-$) and T'(NX_4^+)
			199m, 193w					
		175s	186w, 177s			167m	176m, 169s	T'($XCOO^-$) and T'(NX_4^+)
168sh	187m, 176w			169sh	182w, 169w			T'($XCOO^-$)
	169w							
			159w, 155w				155w, 147w	T'($XCOO^-$)
149s	160s, 151w			154s	159s			L($XCOO^-$)
	139w							
				133s	146s			L($XCOO^-$)
	122vw, 110w	120w	136m, 125m			102w	116m	L($XCOO^-$) and T'(NX_4^+)

[a]Key: s, strong; m, medium; w, weak; vw, very weak; sh, shoulder

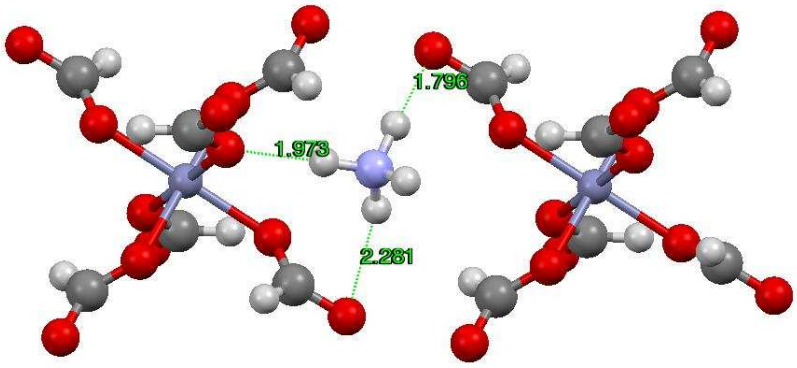

Figure S1. The optimized structure of the NH_4^+ (ND_4^+) cation in the dimeric complex unit (model 1).

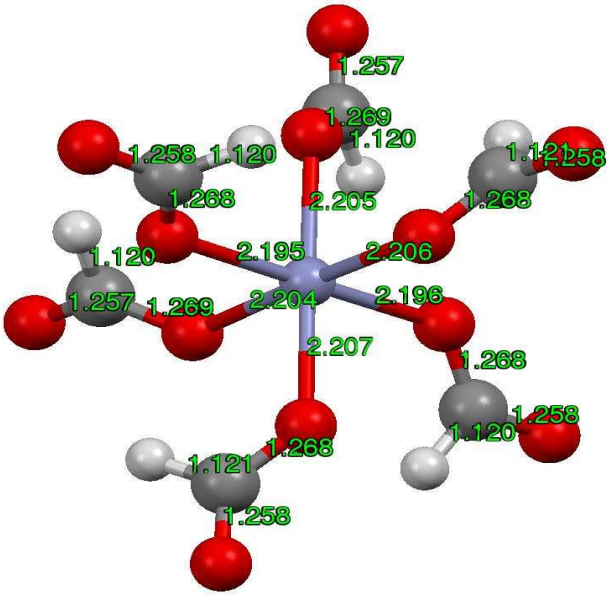

Figure S2. The optimized structure of the monomeric $[Zn(HCOO)_6]^{4-}$ ($[Zn(DCOO)_6]^{4-}$) (model 2).

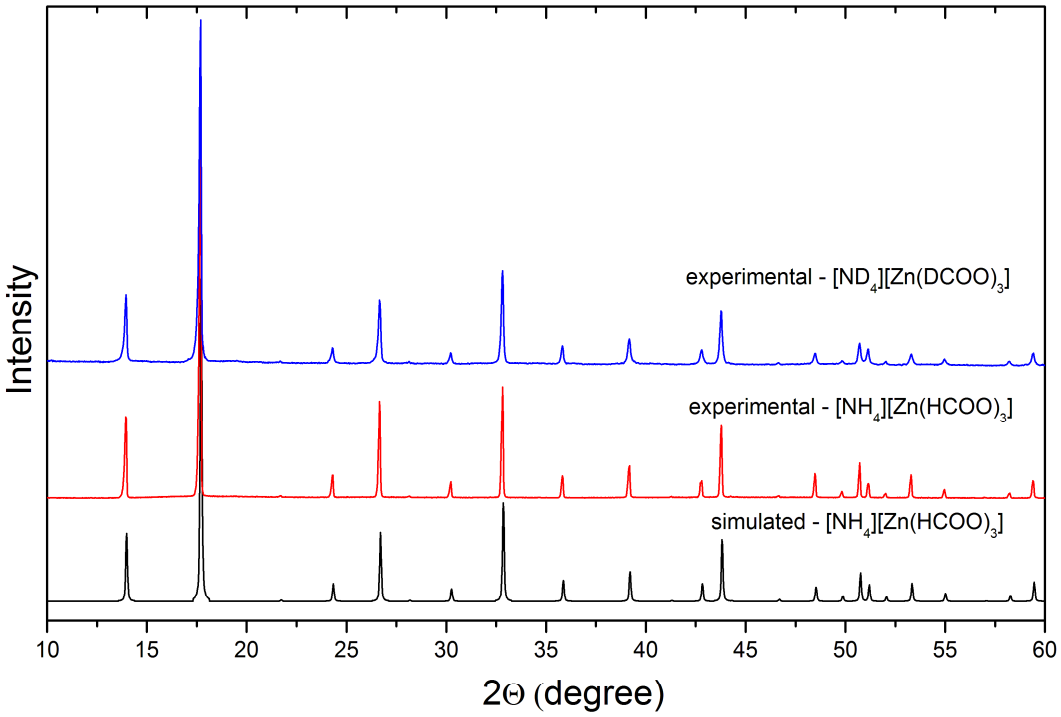

Figure S3. Powder XRD patterns for the as-prepared bulk samples of $[NH_4][Zn(HCOO)_3]$ and $[ND_4][Zn(DCOO)_3]$, with the calculated one based on the single crystal structure of $[NH_4][Zn(HCOO)_3]$.

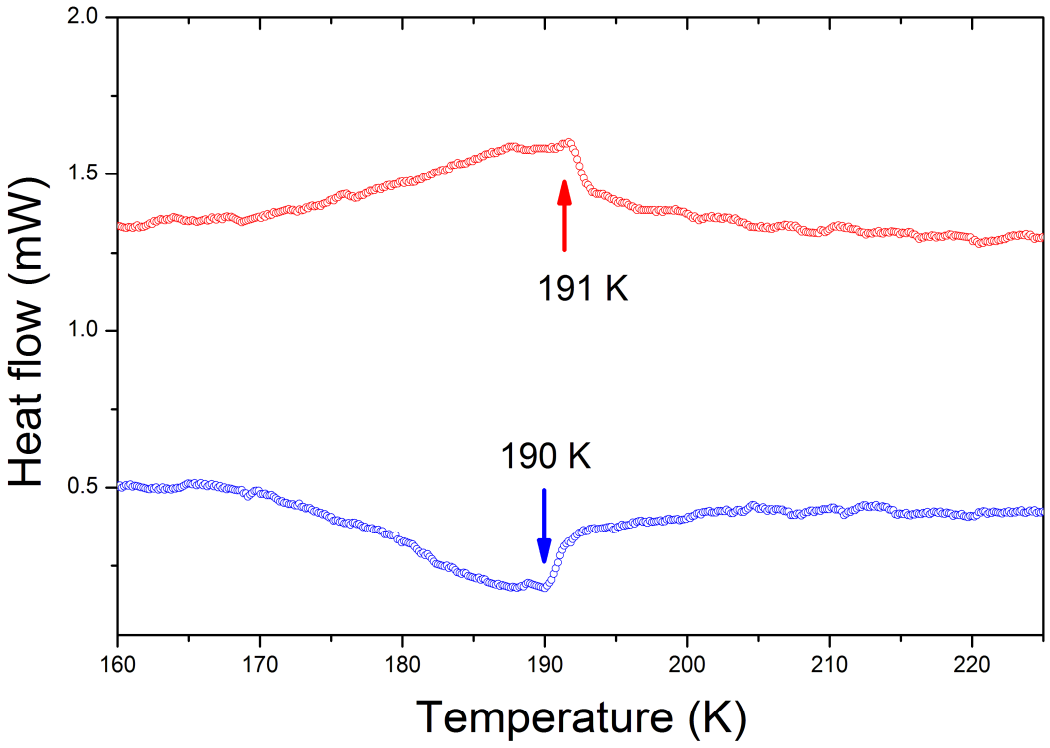

Figure S4. DSC traces for $[ND_4][Zn(DCOO)_3]$ in heating and cooling modes.

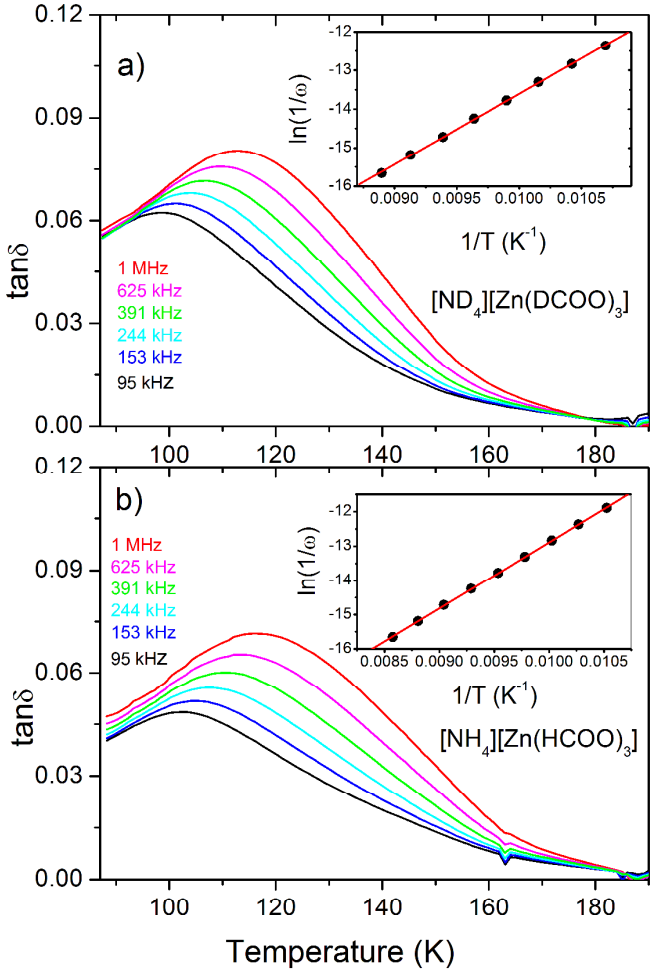

Figure S5. Temperature-dependent traces of tanδ at a few frequencies for powdered (a) $[ND_4][Zn(DCOO)_3]$ and (b) $[NH_4][Zn(HCOO)_3]$. Insets show the Arrhenius plots for the dielectric relaxations.

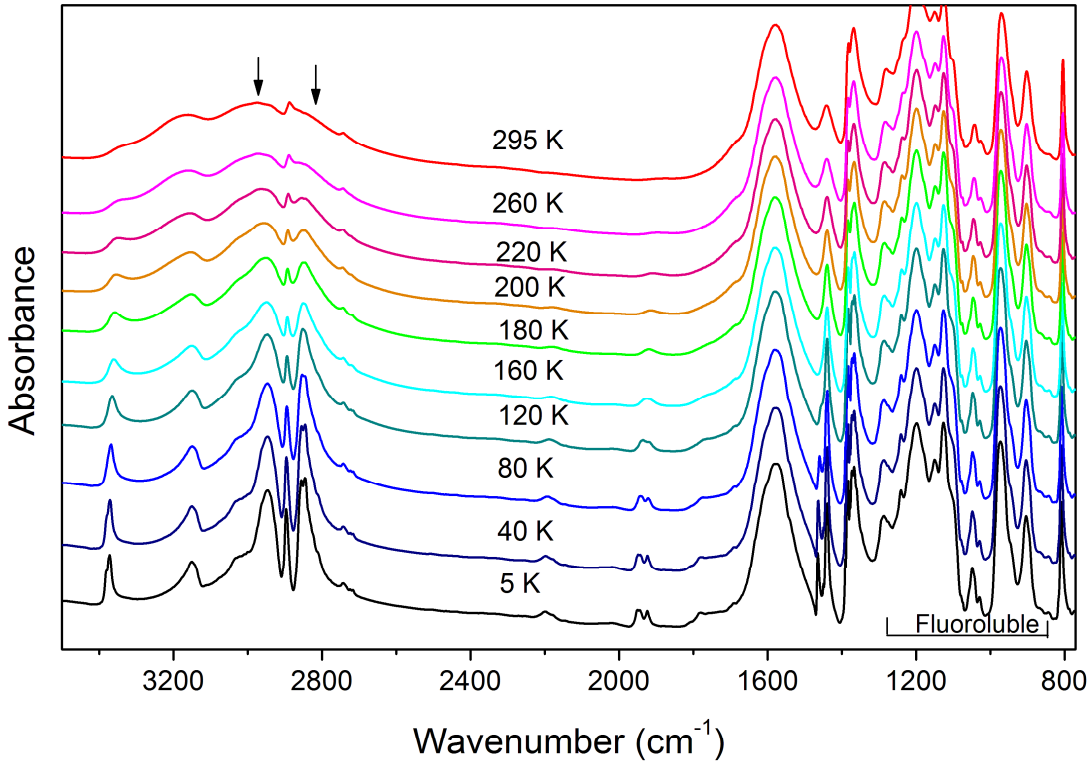

Figure S6. IR spectra of $[NH_4][Zn(HCOO)_3]$ in Fluoroluble suspension recorded at various temperatures corresponding to the spectral range 770-3500 cm^{-1}. Arrows indicate the bands that exhibit pronounced increase in intensity upon cooling.

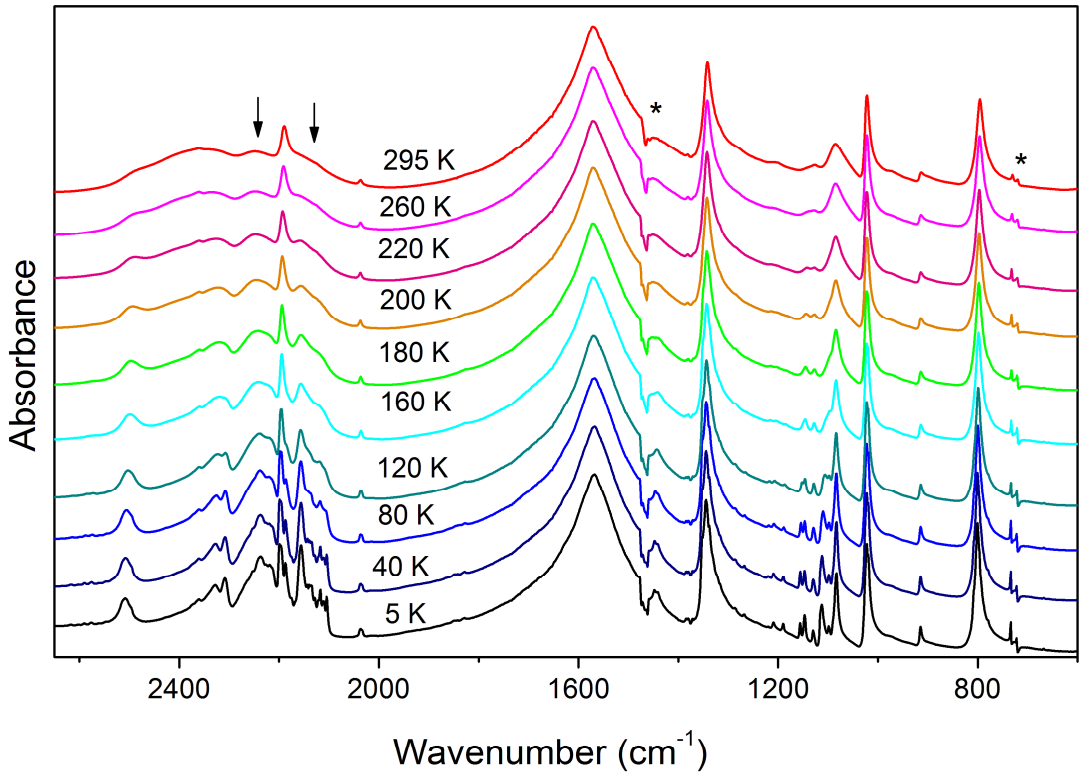

Figure S7. IR spectra of $[ND_4][Zn(DCOO)_3]$ in Nujol suspension recorded at various temperatures corresponding to the spectral range 770-3500 cm^{-1}. Arrows indicate the bands that exhibit pronounced increase in intensity upon cooling. The references spectrum of Nujol was subtracted but some weak features due imperfect correction of the spectra can be still seen, as denoted by the asterisks.

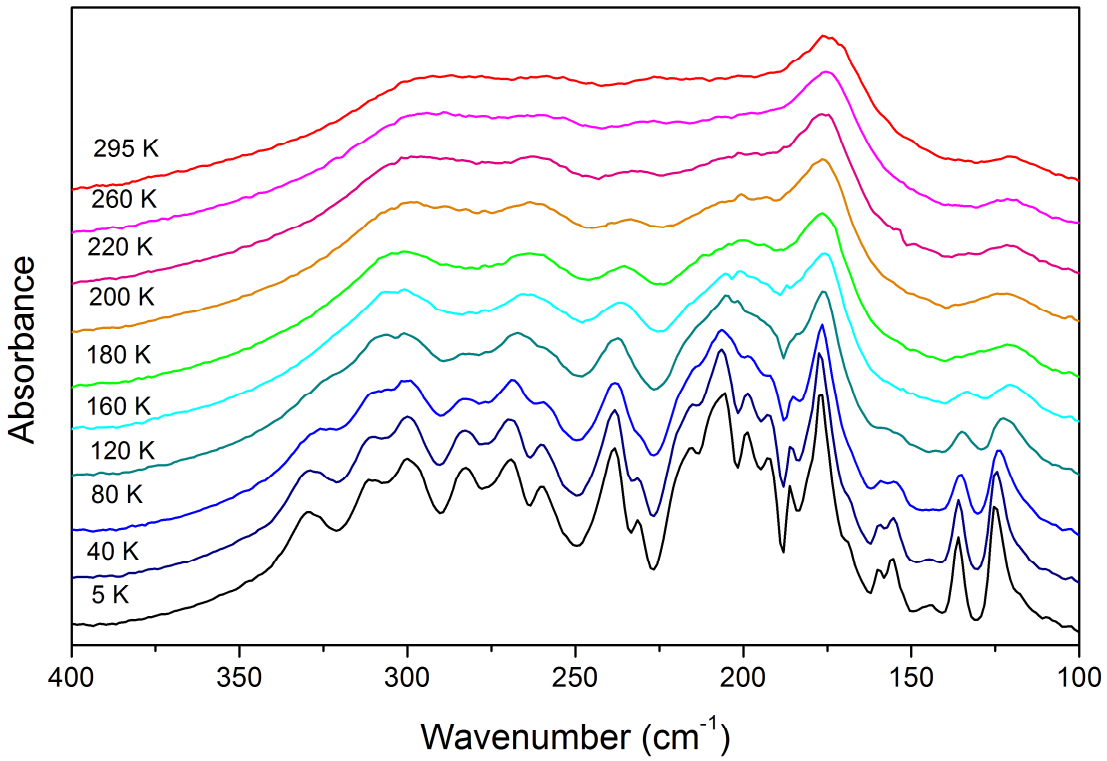

Figure S8. IR spectra of $[NH_4][Zn(HCOO)_3]$ in Apiezon N suspension recorded at various temperatures corresponding to the spectral range 100-400 cm^{-1}.

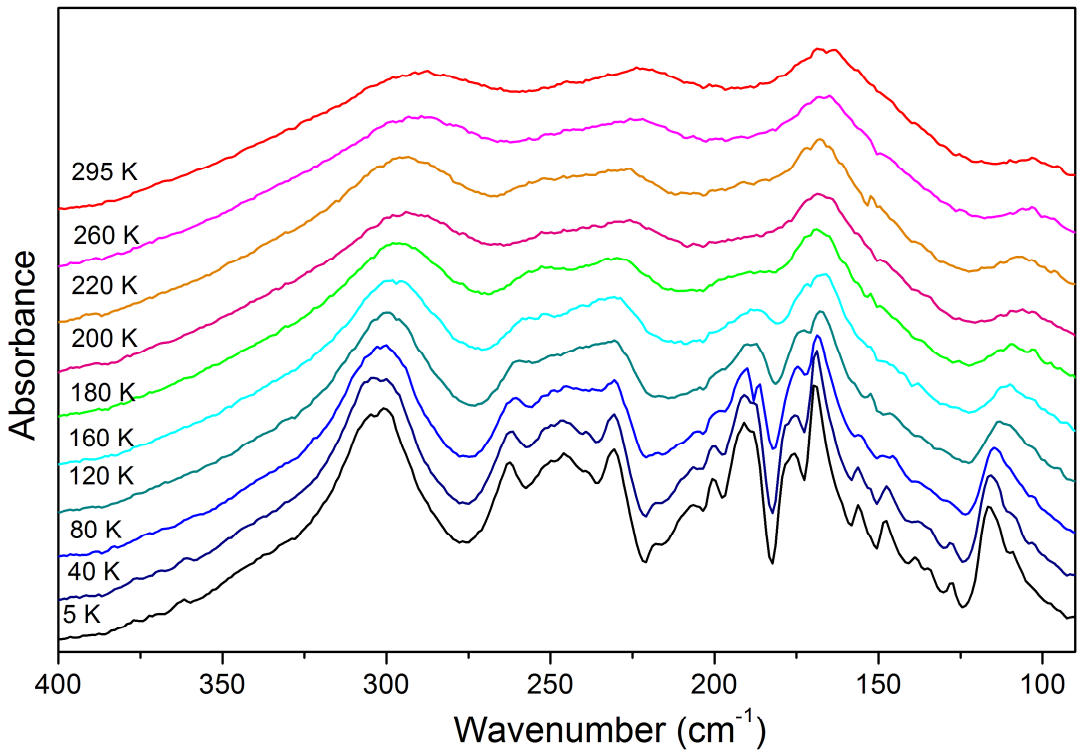

Figure S9. IR spectra of $[ND_4][Zn(DCOO)_3]$ in Apiezon N suspension recorded at various temperatures corresponding to the spectral range 100-400 cm^{-1}.

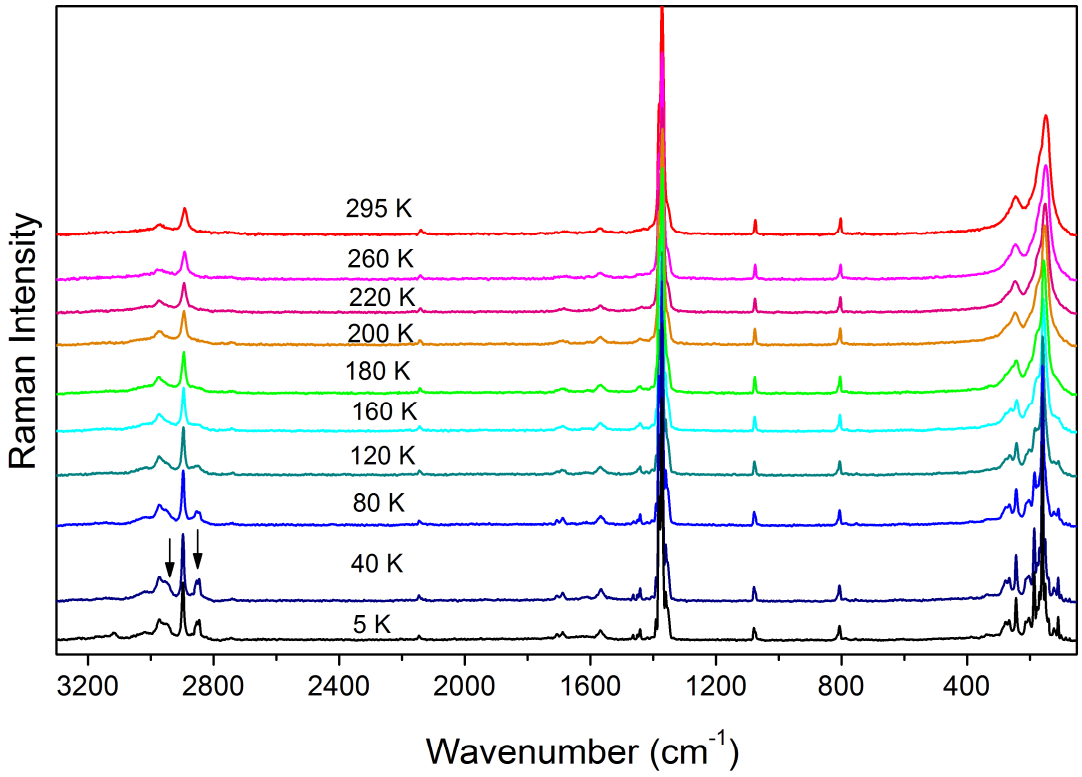

Figure S10. Raman spectra of $[NH_4][Zn(HCOO)_3]$ recorded at various temperatures corresponding to the whole spectral range 50-3300 cm^{-1}. Arrows indicate the bands that exhibit pronounced increase in intensity upon cooling.

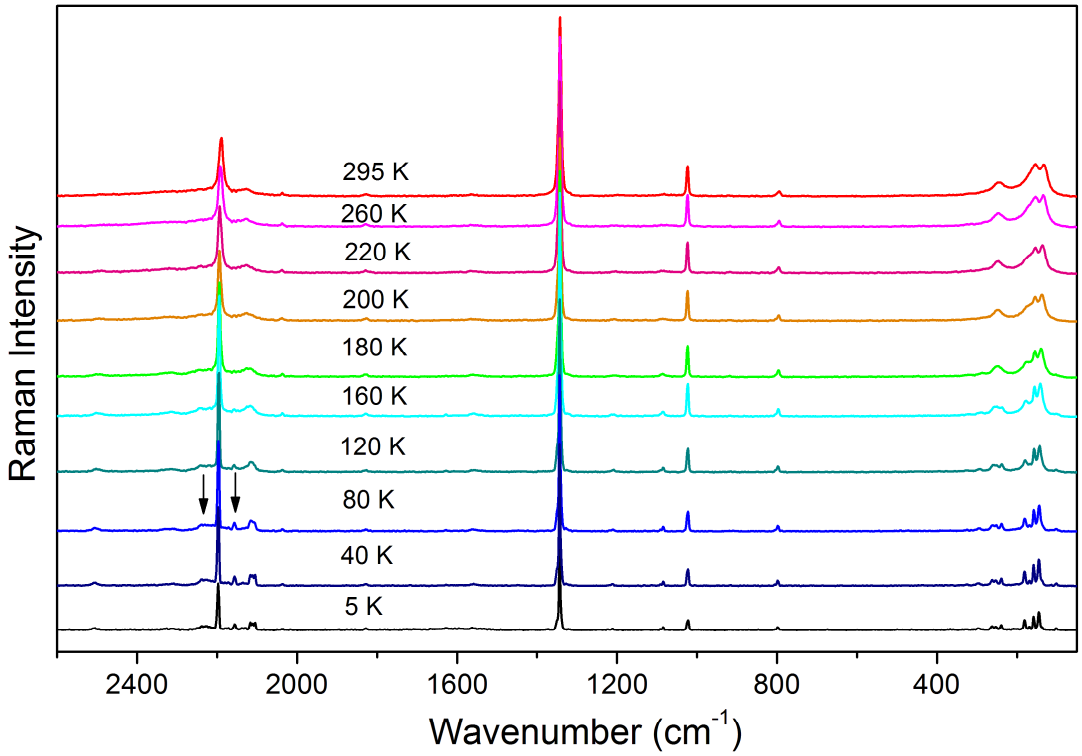

Figure S11. Raman spectra of $[ND_4][Zn(DCOO)_3]$ recorded at various temperatures corresponding to the whole spectral range 50-3300 cm^{-1}. Arrows indicate the bands that exhibit pronounced increase in intensity upon cooling.

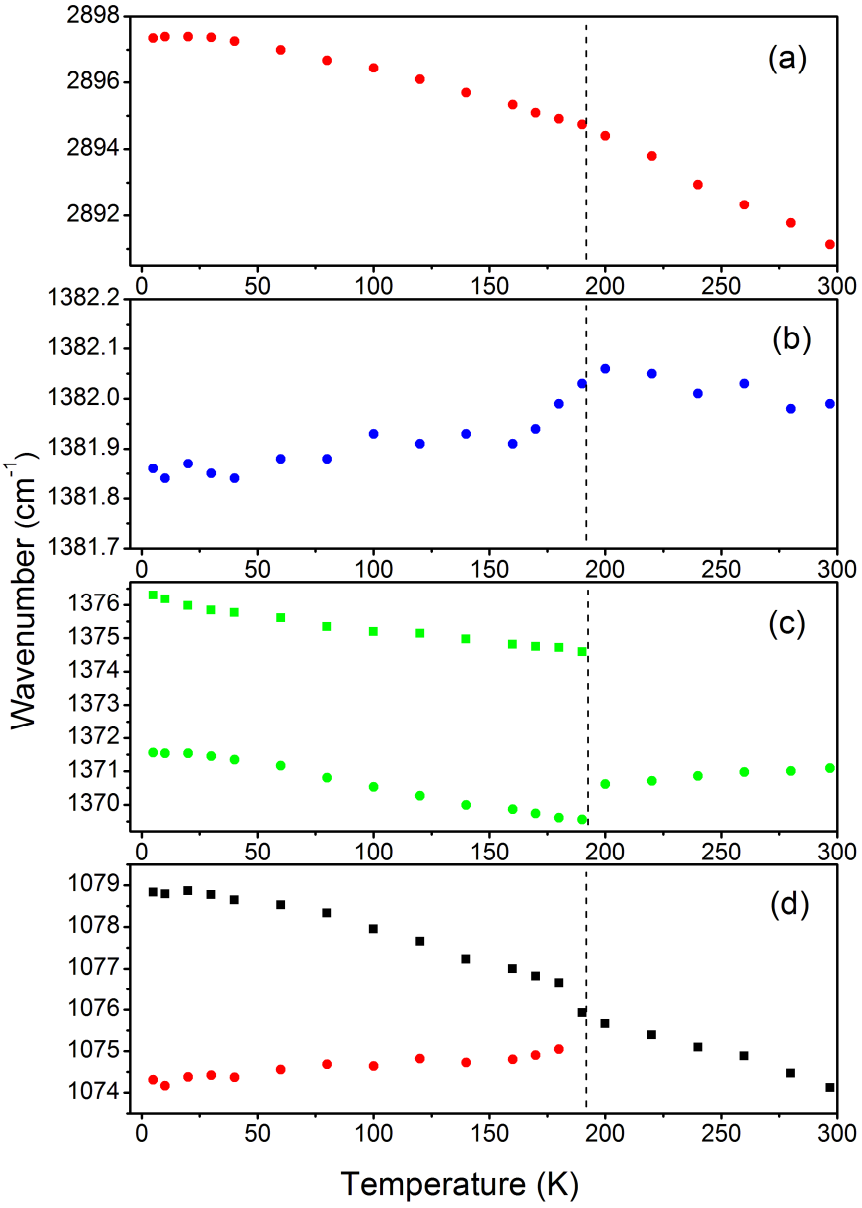

Figure S12. Temperature dependence of the (a) 2891 ($\nu_1(HCOO^-)$), (b) 1382 ($\nu_5(HCOO^-)$), (c) 1371 ($\nu_2(HCOO^-)$) and (d) 1074 cm^{-1} ($\nu_6(HCOO^-)$) Raman bands of $[NH_4][Zn(HCOO)_3]$. The vertical lines indicate the phase transition temperature.

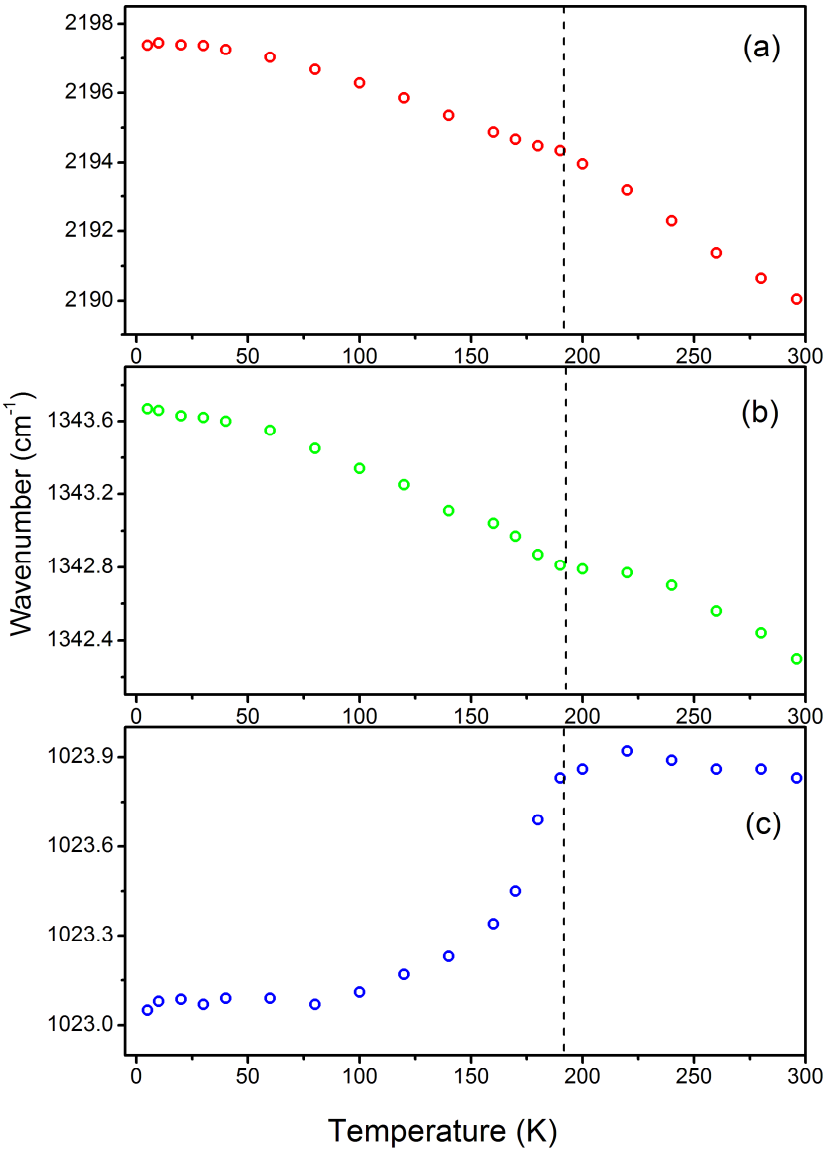

Figure S13. Temperature dependence of the (a) 2190 ($\nu_1(DCOO^-)$), (b) 1342 ($\nu_2(DCOO^-)$) and (d) 1024 cm^{-1} ($\nu_5(DCOO^-)$) Raman bands of $[ND_4][Zn(DCOO)_3]$. The vertical lines indicate the phase transition temperature.

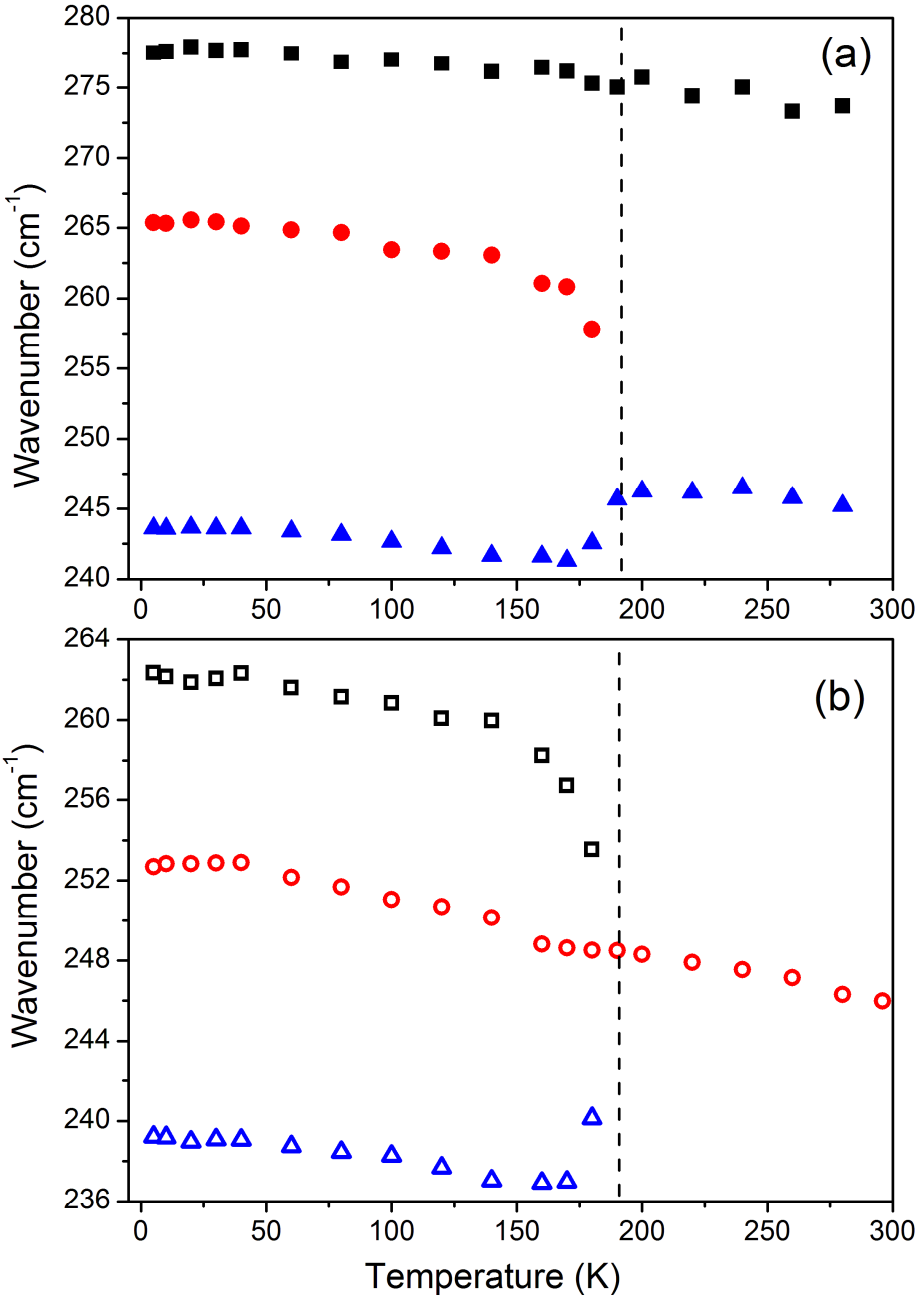

Figure S14. Temperature dependence of the Raman bands near 250 cm^{-1} corresponding to the coupled T'($XCOO^-$) and T'(Zn^{2+}) modes for (a) $[NH_4][Zn(HCOO)_3]$ and (b) $[ND_4][Zn(DCOO)_3]$. The vertical lines indicate the phase transition temperature.

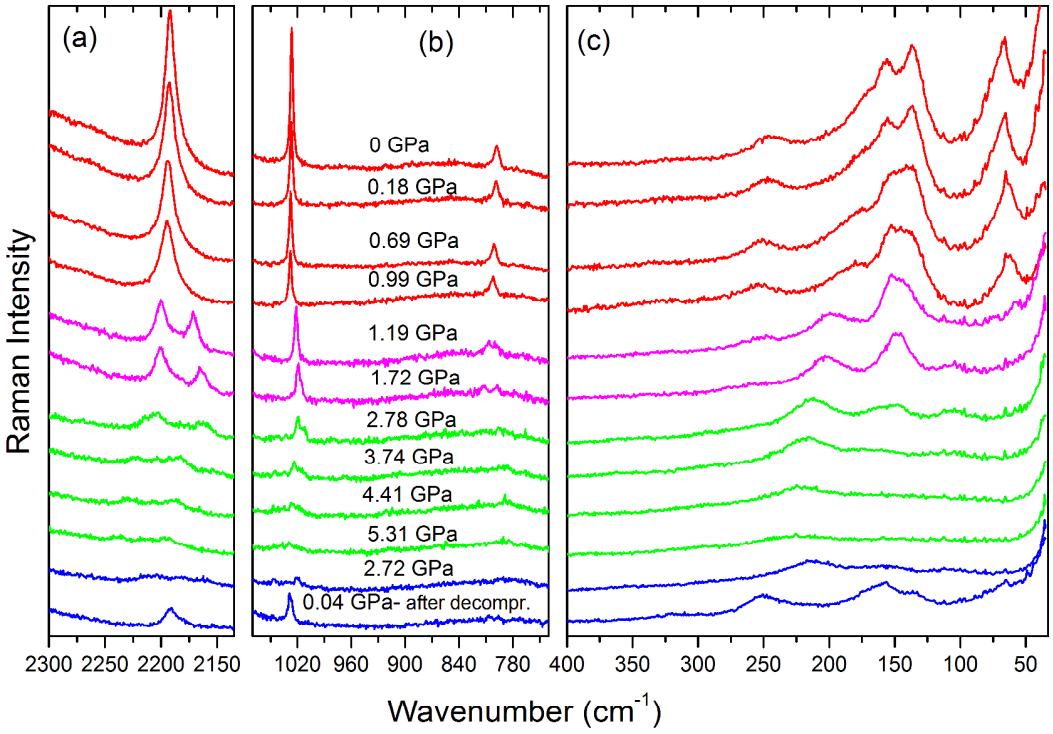

Figure S15. Raman spectra of $[ND_4][Zn(DCOO)_3]$ recorded at different pressures during compression (red, magenta and green) and decompression experiments (blue). Spectra below 1 GPa presented in figures (a) and (b) were divided by two for the comparison sake.

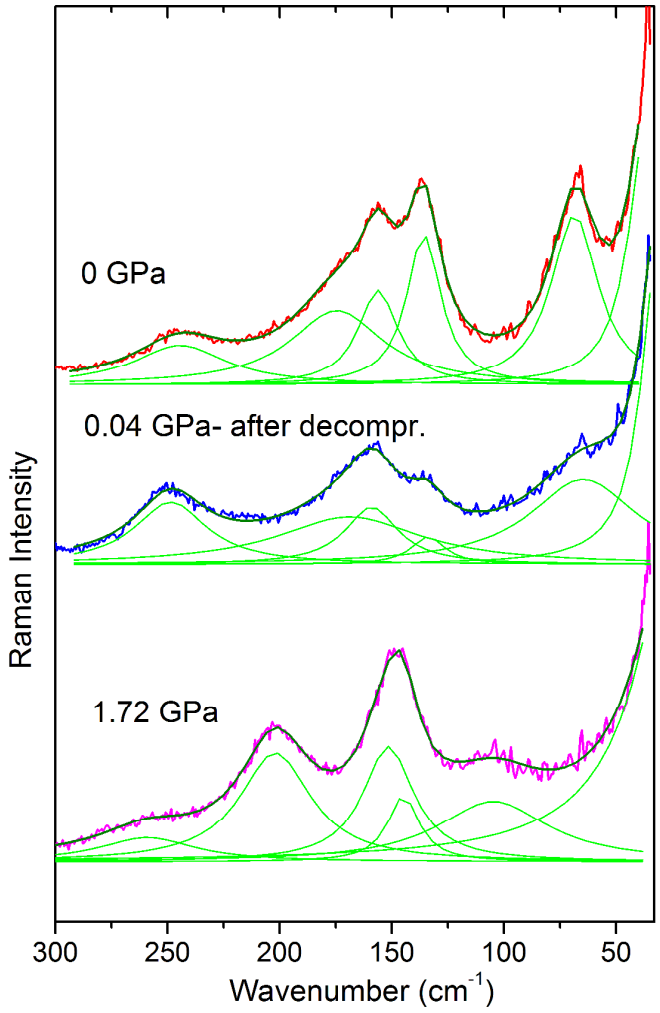

Figure S16. Raman spectra of $[ND_4][Zn(DCOO)_3]$ recorded before compression, after decompression and at 1.72 GPa. The spectrum before compression was divided by four for the comparison sake. The spectra were deconvoluted into Lorenzian components. This comparison shows very clearly that the spectrum after decompression is very different from that corresponding to the high pressure phase measured at 1.72 GPa. Positions of the bands are, however, in good agreement with those observed for the initial phase before compression, although significant changes in relative intensities and bandwidths are evident.